NANO LETTERS

Letter

pubs.acs.org/NanoLett

Polarization-Selective Coupling to Long-Range Surface Plasmon Polariton Waveguides

J. P. Balthasar Mueller,[†] Kristjan Leosson,[‡] and Federico Capasso*[,†]

[†]School of Engineering and Applied Sciences, Harvard University, Cambridge, Massachusetts, United States

[‡]Science Institute, University of Iceland, Reykjavik, Iceland

Supporting Information

ABSTRACT: We demonstrate polarization-selective coupling from an optical fiber to long-range surface plasmon polariton waveguide modes using plasmonic antenna arrays. The arrays allow the sorting of two distinct (not necessarily orthogonal) polarizations to counter-propagating waveguide modes. The polarization-selective behavior of the devices is described by a compact formalism based on Stokes vectors that offers a clear graphical representation of the response. We experimentally observe polarization-controlled switching and unidirectional coupling with extinction ratios greater than 30 dB and coupling efficiencies comparable to those of a conventional grating coupler.

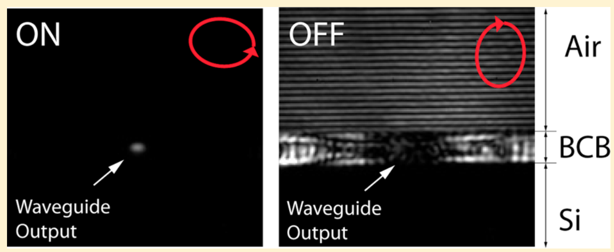

KEYWORDS: *Long-range surface plasmon polaritons, plasmonic antenna arrays, metasurfaces, couplers, beam splitters, polarization-selective devices*

Grating couplers are a prevalent design choice for coupling light to optical waveguides, yet they offer limited control over both the direction of propagation of the coupled optical power in the waveguide as well as over the polarization state that is coupled. Recently, novel coupling schemes were used to couple light to bound electromagnetic waves at a metal—dielectric interface called surface plasmon polaritons (SPPs), which were launched unidirectionally in different directions depending on the circular polarization state of the incident light.[1,2] These couplers, which we may refer to as "meta-gratings," rely on arrays of polarization-selective aperture antennas milled into the metal film, which are spaced and rotated to obtain polarization-sorting properties. As a particular case of a meta-grating, the "Fishbone" (FB) coupler demonstrated by our group[1] has the additional advantage of in principle allowing the coupling of any polarization state on the Poincaré Sphere with equal overall efficiency, thus removing the limitation on the coupled polarization states commonly encountered with previous plasmonic couplers. We demonstrate here for the first time a realization of a Fishbone coupler in a waveguide system and describe deviations in the polarization response that occur with the respect to the "ideal" case that is described in ref 1. The fishbone coupler is furthermore implemented with metal rod antennas rather than apertures in a metal film, which is a configuration that is more readily adaptable to a wide variety of waveguide systems such as dielectric waveguides. To succinctly describe the polarization-sorting properties of the array we introduce a simple formalism based on Stokes vectors that allows for a geometrical representation of the effective response of polarization-selective optical elements. This intuitive picture is useful in the presence of distortions to the response that arise due to defects and reflections when a polarization-selective coupler is integrated in a real-world optical circuit.

As a model system, we employ long-range surface plasmon polariton (LRSPP) waveguides, which consist of nanometer-thin metal strips embedded in a homogeneous dielectric environment.[3] The guided mode of such waveguides corresponds to the symmetric hybrid mode that arises from the coupling of the SPP modes at the top and bottom surfaces of the metal film as the film thickness is decreased, and is always transverse-magnetic (TM) polarized. In contrast to conventional surface plasmon polaritons, LRSPPs can achieve centimeter-scale propagation lengths and enable near-perfect mode-matching to optical fibers,[4] as well as simultaneous guiding of electrical and optical signals.[5] Their simple geometry enables straightforward and highly reproducible fabrication using standard methods, which in combination with the possibility of thermo-optic fine-tuning,[5] absence of polarization noise and lower pump noise renders LRSPPs an excellent platform for specialized applications in high-precision optics.[6,7]

Our waveguides consist of 10 μm wide Au stripes with a thickness of 15 nm that are embedded in benzocyclobutene (BCB) polymer (Figure 1a), which has a refractive index of n_{BCB} = 1.535 at 1550 nm. This geometry supports a single TM-polarized mode at C and L band frequencies (λ_0 = 1530 to 1625 nm), covering the "erbium window" commonly used in optical communications. Waveguides were patterned with UV-

Received: May 20, 2014
Revised: August 12, 2014
Published: August 25, 2014

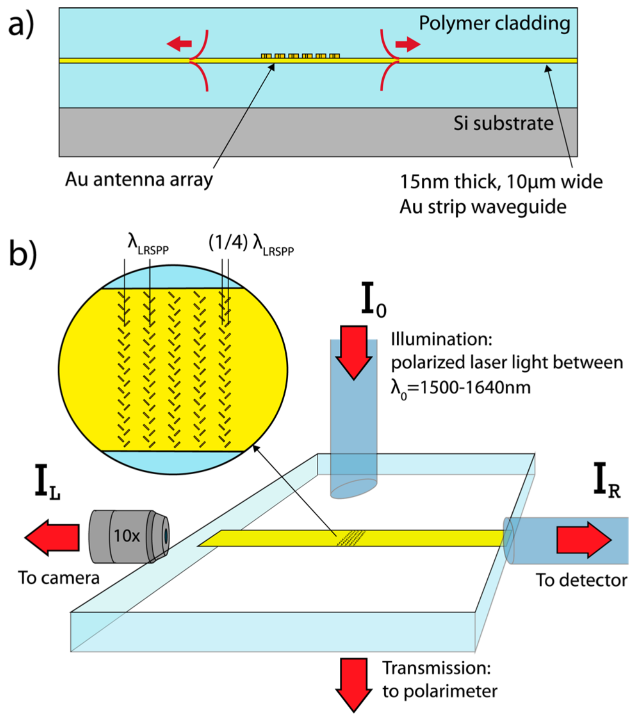

Figure 1. (a) Side view of a gold long-range surface plasmon polariton (LRSPP) waveguide patterned on top of a polarization-sorting gold antenna array. Under illumination, the antenna array launches LRSPPs propagating to the left and to the right toward the waveguide end-facets. (b) The polarization response of the devices is measured by observing the light output at the waveguide end-facets as the coupler is illuminated with light of variable polarization from an optical fiber. The output is monitored both by using a camera and an optical fiber that leads to a photodetector. Inset: Top-view of the LRSPP waveguide with FB coupler designed for operation at an LRSPP wavelength of λ_{LRSPP}.

lithography on top of antenna arrays consisting of subwavelength-spaced rows of 200 nm long, 80 nm wide, and 15 nm thick Au rod antennas fabricated with electron-beam lithography. The rows are arranged in pairs with lateral spacing of $\lambda_{\mathrm{LRSPP}}/4$ with the antennas oriented at $\pm 45°$ with respect to the waveguide axis and with 10 row pairs patterned a distance of $\lambda_{\mathrm{LRSPP}} \approx \lambda_0/n_{\mathrm{BCB}}$ apart to increase the overall cross-section of the coupler (Figure 1b, inset). The circular-polarization-sorting properties of this configuration emerge as the rows with antennas at $\pm 45°$ orientation couple to mutually orthogonal linear polarization states of the incident light and launch LR SPPs that interfere constructively only in one direction for circularly polarized light due to the temporal and propagation phase-delays between the rows. This mechanism is described in detail in ref 1 and provides a robust and scalable scheme for designing polarization-selective couplers.

The fabricated devices were characterized using light from a fiber-coupled tunable laser source (Tunics Plus) with a cleaved end of the fiber (SMF28) end-fire coupled to the antenna arrays at normal incidence. The waveguide output was observed at the end-facets of the sample with an InGaAs camera (Hamamatsu) or picked up and detected with an optical fiber coupled to a photodetector (Figure 1b). The polarization of the light incident on the antenna array was adjusted with a manual polarization controller and continuously monitored in transmission with a polarimeter (Thorlabs) positioned behind the sample.

The previously demonstrated Fishbone coupler[1] was characterized using direct imaging of the launched SPPs using near-field scanning optical microscopy, which did not yield quantitative information about the intensity of the launched SPPs. In the present case, we wish to describe the device response in terms of the optical power routed to the left and the right propagating SPP channel as a function of the incident polarization. To do so, we consider that the action of any polarization selective device may be described in terms of projective measurements of a vector describing the polarization of the incident light, such as a Stokes vector, which offers the advantage of a description of light in terms of directly measurable quantities.[8] The Stokes vector describing a fully polarized beam is given by $\vec{S} = I_0[1,\hat{s}]^T$, where superscript ^{T} denotes the matrix transpose, I_0 is the intensity of the beam, and $\hat{s} = [S_1/S_0, S_2/S_0, S_3/S_0]^T$ is a three-dimensional unit vector describing the state of polarization (SOP), where $S_0 ... S_3$ are the four Stokes parameters of the incident light.[8] The SOP of light corresponds to the coherent superposition of two orthogonal polarization states, so that the possible values of $\hat{s}$ can be conveniently graphically represented as points on the surface of a sphere. This type of geometric representation of a two-level system is known as Bloch sphere in solid state physics and as the Poincaré sphere in optics.

The response of any real device will be subject to deviations from the ideal case, for example due to fabrication defects and internal reflections. To account for this, we separately consider the response of the left and right waveguide outputs as independent channels. They each couple to some polarization that is described by Stokes vectors ("device vectors") $D_{\mathrm{R}} = c_{\mathrm{R}}[1,\hat{d}_{\mathrm{R}}]^T$ and $D_{\mathrm{L}} = c_{\mathrm{L}}[1,\hat{d}_{\mathrm{L}}]^T$, where $c_{\mathrm{R,L}}$ in this case are coupling efficiencies and $\hat{d}_{\mathrm{R,L}}$ describe the coupled SOP on the Poincaré Sphere.[7] The left and right output intensities I_{L} and I_{R} are then given by the respective projections of the Stokes vector describing the incident light S along the device vectors, that is, $I_{\mathrm{R}} = S \cdot D_{\mathrm{R}}$ and $I_{\mathrm{L}} = S \cdot D_{\mathrm{L}}$.

The device vectors D_{L} and D_{R} can be measured by adjusting the incident SOP $\hat{s}$ to three different polarizations $\hat{m}_i$ (for example left circularly, horizontally linearly, and diagonally linearly polarized) while recording the output power. For each polarization m_i, the output intensity $I_{\mathrm{R,L}}^{(i)}$ on the right or the left channel is given by

$$I_{\mathrm{R,L}}^{(i)} = I_0 c_{\mathrm{R,L}}[1 + \hat{m}_i \cdot \hat{d}_{\mathrm{R,L}}] \quad (1)$$

This enables us to write a linear system for the SOP of the device vectors $\hat{d}_{\mathrm{R,L}}$

$$\vec{I} = I_0 c[\vec{1} + M\hat{d}] \quad (2)$$

where $\vec{I} = [I^{(1)}, I^{(2)}, I^{(3)}]^T$, $\vec{1} = [1,1,1]^T$ and

$$M = \begin{bmatrix} \cdots & m_1 & \cdots \\ \cdots & m_2 & \cdots \\ \cdots & m_3 & \cdots \end{bmatrix} \quad (3)$$

is a matrix containing the three incident polarizations m_i used in the measurement as rows. The subscripts indicating the left- or right channels R,L were omitted for clarity. The SOP of the device vectors $\hat{d}$ is found by solving

$$\hat{d} = M^{-1}\left[\frac{\vec{I}}{I_0 c} - \vec{1}\right] \quad (4)$$

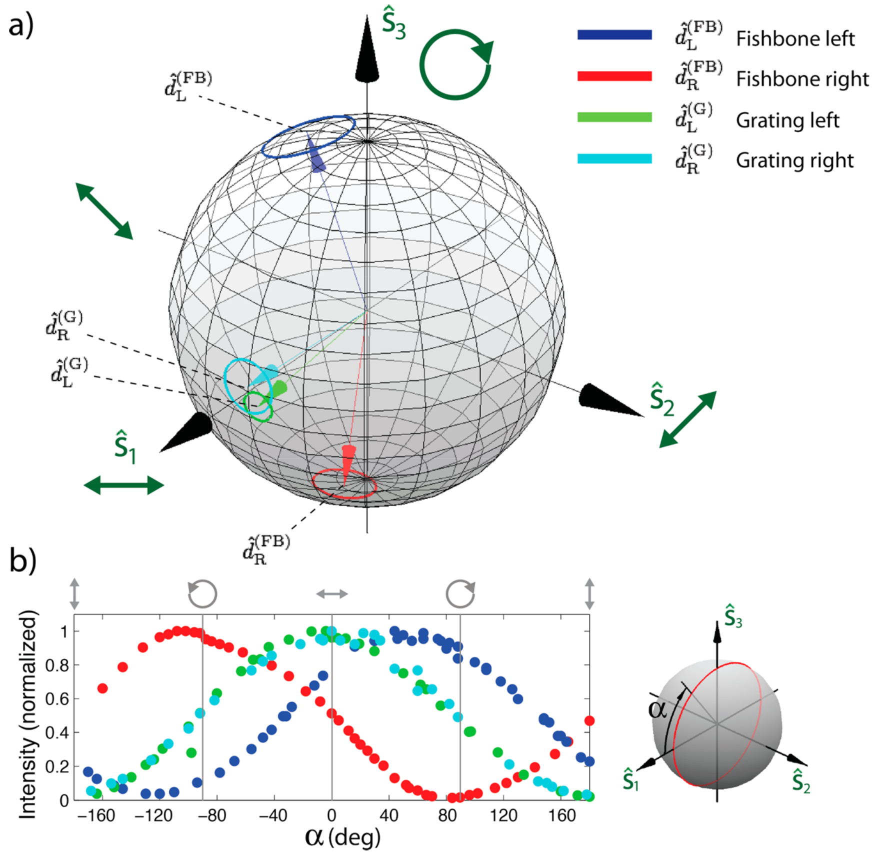

Figure 2. (a) The device vectors corresponding to the left (dark blue) and right (red) output channels of the structure on the Poincaré Sphere. The device vectors of the left and right output of a conventional grating coupler are shown in green and light blue. The standard deviation for measurements of the device vector over the measured wavelength window is shown as circles on the surface of the sphere. (b) Left (dark blue) and right (red) output intensities from the structure as the polarization of the incident light at 1550 nm is varied to trace out a great circle on the Poincaré Sphere in the S_1,S_3 plane (inset), where the horizontal linear polarization (S_1) is taken to be parallel to the waveguide axis. The linear and circular polarization states are marked in gray. The maximal output of the left and right output channels respectively deviate from the circularly polarized states by ca. 22° and 10°. The left and right outputs of a conventional grating coupler are plotted in green and light blue, respectively.

where superscript $^{-1}$ denotes the matrix inverse. The maximum coupling efficiency that is obtained when the input polarization is directly aligned with the device vectors, c, can be found by recognizing that $\hat{d}\cdot\hat{d} = 1$ and choosing the positive root of the resulting quadratic equation, that is

$$c = \frac{1}{I_0}\left[\frac{2\alpha}{-\beta + \sqrt{\beta^2 - 4\alpha\gamma}}\right] \tag{5}$$

where $\alpha = (M^{-1}\vec{I})^T M^{-1}\vec{I}$, $\beta = (M^{-1}\vec{I})^T M^{-1}\vec{1} + (M^{-1}\vec{I})^T$ and $\gamma = (M^{-1}\vec{1})^T M^{-1}\vec{1} - 1$. It is worth emphasizing that the device vectors capture the effective source-to-detector coupling efficiency and polarization response of the entire system, which are the relevant quantities for an actual integration of the device. As such, they are subject not only to the response of the coupler by itself, but also to the alignment of the optical fibers at the input and output of the devices, fiber losses, reflections, and other factors. This is in particular true for the effective coupling efficiency c, which is extremely sensitive to alignment.

Figure 2a shows the device vectors of the left and right output channels of a Fishbone coupler and a conventional grating coupler designed for operation around 1550 nm determined using this approach. The device vectors of the structure exhibit only weak wavelength dependence over the entire C and L bands, consistent with simulations indicating a large bandwidth for conventional LRSPP grating couplers based on metal films with a modulated thickness.[8] Figure 2b displays the normalized left and right outputs of the devices as the input polarization was traced along a great circle around the Poincaré Sphere corresponding to the intersection of the sphere with the S_1,S_3-plane (Figure 2b inset). As expected, the output undergoes a sinusoidal variation corresponding to the projection of the input Stokes vector S on the device vectors. Notably, channels can be switched off by choosing the input polarization to be orthogonal to the corresponding device vector while the output on the opposite channel remains finite. This allows signals to be unidirectionally coupled to only one of the output channels with the unidirectionally coupled polarization states $\hat{u}_{R,L}$ satisfying $\hat{u}_R\cdot\hat{d}_L = -1$ and $\hat{u}_L\cdot\hat{d}_R = -1$. Any other incident polarization state results in a division of the total coupled intensity between the left and right output channel according to $I_R = S\cdot D_R$ and $I_L = S\cdot D_L$. We observed unidirectional coupling with extinction ratios of at least 30 dB, limited by the noise threshold of our measurement (Figure 3).

Consistent with the weak wavelength-dependence of the device vectors, we did not observe any significant shifts in the wavelength-dependent coupling efficiency for antenna arrays that had row spacings designed for operation at wavelengths between 1550 and 1610 nm. This indicates that the response of the gratings themselves is relatively flat and grating effects do

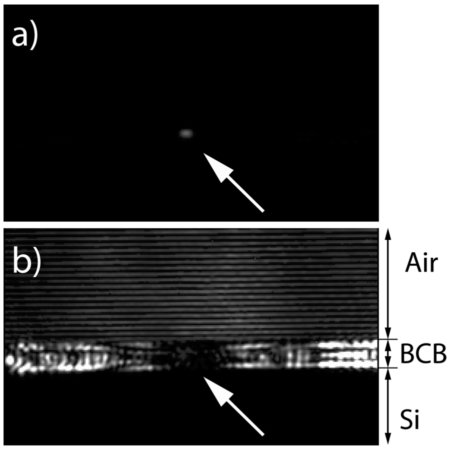

Figure 3. (a) Camera image of one waveguide output for polarization aligned with the device vector ($\hat{s} \approx \hat{d}$), showing single-mode output from the waveguide end-facet. (b) Camera image of the same waveguide output for polarization orthogonal to the device vector ($\hat{s} \approx -\hat{d}$), showing no measurable output from the waveguide end-facet. For this image, both laser power and camera exposure time were maximized to increase signal, which renders scattered light that is propagating above the sample in air and within the BCB polymer cladding visible. The fringes visible in the air above the BCB result from Lloyd's mirror-type interference of light from the fiber that is diffracted toward the camera.

not play a dominant role over the measured wavelength range. The measured wavelength response is however significantly modulated in a manner consistent with interference in the BCB layer that is caused by internal reflections at the Au−BCB and BCB−Si interfaces, which results in a rapid fluctuation of the coupling efficiency as a function of wavelength (see the Supporting Information). The details of the wavelength response over a wider range of wavelengths will be reported elsewhere. The maximum efficiency of our polarization-selective couplers was observed to be close to that of a conventional grating coupler on the same type of waveguide, using ridges with the same width (80 nm) and height (15 nm) as for the individual rod antennas and the same grating period. This is indicates that the Fishbone couplers should in principle be able to perform with similar efficiency as grating couplers, which have been extensively studied in the literature. While the very shallow antennas were designed to provide weak coupling (<1%) to the plasmonic mode, we expect that the efficiency of the Fishbone couplers can be significantly increased by optimizing in particular the resonant properties of individual antennas.[9]

In conclusion, we have demonstrated polarization-selective coupling to LRSPP waveguide modes by implementing a recently developed coupling scheme for the first time in an integrated waveguide system. The system is capable of polarization-sorting to two counter-propagating output channels, enabling in particular polarization-controlled unidirectional coupling. The effective polarization response of the device can be accurately described and graphically represented with vectors analogous to Stokes vectors describing the state of a light beam. The enhanced control over the coupling to waveguide systems may pave the way towards a new class of optical switches and polarization splitters for integrated optical networks, as well as for novel experiments in quantum optics.

■ ASSOCIATED CONTENT

Ⓢ Supporting Information

Wavelength dependence of the coupling efficiency. This material is available free of charge via the Internet at http://pubs.acs.org.

■ AUTHOR INFORMATION

Corresponding Author

*E-mail: capasso@seas.harvard.edu.

Author Contributions

The manuscript was written through contributions of all authors. All authors have given approval to the final version of the manuscript.

Notes

The authors declare no competing financial interest.

■ ACKNOWLEDGMENTS

The authors thank Virginia Merk and Rögnvaldur Líndal Magnússon for assistance with the fabrication of the waveguides and the realization of the experimental setup. This work was supported by the Airforce Office of Scientific Research (AFOSR) under Grant FA9550-12-1-0289 and the University of Iceland Research Fund.

■ REFERENCES

(1) Lin, J.; Mueller, J. P. B.; Wang, Q.; Antoniou, N.; Yuan, X.-C.; Capasso, F. Polarization-Controlled Tunable Directional Coupling of Surface Plasmon Polaritons. *Science* **2013**, *340* (6130), 331−334.

(2) Huang, L.; Chen, X.; Bai, B.; Tan, Q.; Jin, G.; Zentgraf, T.; Zhang, S. Helicity dependent directional surface plasmon polariton excitation using a metasurface with interfacial phase discontinuity. *Light Sci. Appl.* **2013**, *2* (3), e70.

(3) Berini, P. Plasmon polariton modes guided by a metal film of finite width. *Opt. Lett.* **1999**, *24* (15), 1011−1013.

(4) Nikolajsen, T.; Leosson, K.; Salakhutdinov, I.; Bozhevolnyi, S. I. Polymer-based surface-plasmon-polariton stripe waveguides at telecommunication wavelengths. *Appl. Phys. Lett.* **2003**, *82*, 668.

(5) Nikolajsen, T.; Leosson, K.; Bozhevolnyi, S. I. Surface plasmon polariton based modulators and switches operating at telecom wavelengths. *Appl. Phys. Lett.* **2004**, *85*, 5833.

(6) Leosson, K. Optical amplification of surface plasmon polaritons: review. *J. Nanophotonics* **2012**, *6* (1), 061801.

(7) Zhang, T.; Qian, G.; Wang, Y.-Y.; Xue, X.-J.; Li, R.-Z.; Wu, J.-Y.; Zhang, X.-Y. Integrated optical gyroscope using active Long-range surface plasmon-polariton waveguide resonator. *Sci. Rep.* **2014**, *4*, 3855.

(8) Damask, J. N. *Polarization Optics in Telecommunications*; Springer Series in Optical Sciences; Springer: New York, 2005.

(9) Chen, C.; Berini, P. Grating couplers for broadside input and output coupling of long-range surface plasmons. *Opt. Exp.* **2010**, *18* (8), 8006−80018.